International Journal of Heat and Mass Transfer 52 (2009) 2858–2870

Contents lists available at ScienceDirect

International Journal of Heat and Mass Transfer

journal homepage: www.elsevier.com/locate/ijhmt

# Turbulent natural convection of sodium in a cylindrical enclosure with multiple internal heat sources: A conjugate heat transfer study

Anil Kumar Sharma [a], K. Velusamy [a], C. Balaji [b,*]

[a] Indira Gandhi Center for Atomic Research, Department of Atomic Energy, Kalpakkam 603 102, India
[b] Heat Transfer and Thermal Power Laboratory, Department of Mechanical Engineering, Indian Institute of Technology Madras, Chennai 600 036, India

ARTICLE INFO

*Article history:*
Received 16 April 2008
Received in revised form 4 November 2008
Available online 7 February 2009

*Keywords:*
Turbulent natural convection
Low Prandtl number fluid
Fast reactor
Distributed heat source
Numerical simulation
Water experiments

ABSTRACT

Turbulent natural convection of liquid metal in a cylindrical enclosure with locally distributed heat source has been investigated for Boussinesq number in the range of $4.5 \times 0^{11}$– $6.25 \times 10^{12}$. The enclosure considered is an ideal model of the lower plenum of a fast reactor with tray(s) holding damaged core debris, which continuously generate heat. The focus of the study has been to assess the heat dissipation capacity of single and multiple trays in respecting the specific temperature limits on the tray(s). Heat conduction in the metallic trays and in the impervious core debris mixture and turbulent natural convection of the liquid sodium are solved as a conjugate heat transfer problem. The equations that govern the various heat transfer processes in 2-D axi-symmetric cylindrical polar coordinate system have been solved by the finite volume method. Turbulence has been modeled by the $k$–$\varepsilon$ turbulence model, without the use of wall functions. The predictions of the numerical model have been validated against benchmark data reported in open literature. Also, experiments have been conducted in an ideal water model towards validation of the computational model. For typical enclosure dimensions representing a 500 MWe fast reactor, it is seen that the critical parameters are heat dissipation area of the source (area of trays) and the thickness of the heat source (debris thickness). With increase in the number of trays, the heat transfer area increases while the debris thickness reduces. Both these effects lead to reduction in the tray as well as source temperatures. The heat dissipation capacity exhibits a non-linear relationship with the number of plates.



## 1. Introduction

With increased awareness about global warning and its consequences due to green house gases emitted by thermal power plants, there is renewed interest towards nuclear power, all over the world. In this direction, fast breeder nuclear reactors are likely to contribute significantly in the immediate future due to their strong potential for effective utilization of uranium resource. Liquid sodium is the proven candidate coolant in a fast reactor due to its high boiling point, which leads to a low pressure system and large heat transfer coefficient that is essential to remove very high heat flux encountered in the core and to have a compact reactor size. The focus in the design of future reactors of this type is to have passive features that promote safety and economy. Natural convection is an important ingredient of passive safety features. Analysis of a severe accident leading to meltdown of the whole core is an essential step in the safety evaluation of a nuclear reactor. During such an accident, which occurs due to mismatch between heat generation and heat removal, the core fragments into fine particles, sometimes called as 'core debris' when the molten fuel comes into contact with liquid sodium. These particles continue to generate heat due to the decay of fission products, which is termed as 'decay heat'. This debris has to be accommodated in trays located at the bottom of the reactor core within the primary vessel. These trays are known as core catcher plates. During such an accident, it has to be ensured that the temperature of the primary vessel does not exceed certain specific limits, as the mechanical stress in the vessel due to the weight of its internals is large. But, the temperature of the core catcher plate can be higher as the mechanical load on it is less. The core catcher maintains the damaged core in sub-critical configuration and protects the primary weasel against very high temperature. An innovative concept in core catcher design is having multiple trays that enhance the heat transfer area and reduces debris-bed thickness. The present investigation deals with an idealized model of this problem.

In a pool type fast reactor, the bottom part of the primary vessel and the core support structure form a cylinder enclosure as shown in Fig. 1. Core catcher plates with heat generating core debris are housed inside this enclosure. The heat generated in the debris is dissipated to the cold pool by natural convection of sodium within the enclosure. During this process it has to be ensured that (i) the

* Corresponding author. Tel.: +91 44 22574689; fax: +91 44 225770509.
*E-mail address:* balaji@iitm.ac.in (C. Balaji).

0017-9310/$ - see front matter © 2009 Elsevier Ltd. All rights reserved.
doi:10.1016/j.ijheatmasstransfer.2008.11.021

**Nomenclature**

| | |
|---|---|
| Bo | Boussinesq number (=βg q‴ $H^5/K_{Na}\ \alpha^2_{Na}$) |
| $C_p$ | isobaric specific heat of the fluid, J/kg K |
| $C_\mu$, $C_1$, $C_2$, $C_3$ | constants of the turbulence model |
| $D$ | diameter of the enclosure, m |
| $g$ | acceleration due to gravity, 9.81 m/s$^2$ |
| $H$ | height of the enclosure, m |
| $G_k$ | buoyant production of turbulent kinetic energy, kg/m s$^3$ |
| $K$ | thermal conductivity, W/m K |
| $k$ | turbulent kinetic energy, m$^2$/s$^2$ |
| $q''$ | average convective heat flux, W/m$^2$ |
| $q'''$ | volumetric heat generation rate, W/m$^3$ |
| $P_k$ | shear production of turbulent kinetic energy, kg/m s$^3$ |
| Pr | Prandtl number, ν/α |
| Ra | Rayleigh number (=βg q‴ $H^5/K_{Na}\ \alpha_{Na}\nu$) |
| $T$ | temperature, K |
| $\Delta t$ | numerical time step, s |
| $u$ | radial velocity components, m/s |
| $v$ | axial velocity component, m/s |
| $r$, z | radial and axial coordinate, m |

*Greek symbols*

| | |
|---|---|
| $\alpha$ | thermal diffusivity, m$^2$/s |
| $\beta$ | isobaric cubical expansion coefficient of fluid, K$^{-1}$ |
| $\varepsilon$ | dissipation rate of k, m$^2$/s$^3$ |
| $\mu$ | dynamic viscosity of the fluid, Ns/m$^2$ |
| $\mu_t$ | turbulent viscosity, Ns/m$^2$ |
| $\nu$ | kinematic viscosity of fluid, m$^2$/s |
| $\rho$ | density, kg/m$^3$ |
| $\sigma_k$, $\sigma_T$, $\sigma_\varepsilon$ | turbulent Prandtl numbers of $k$, T and $\varepsilon$ |

*Subscripts*

| | |
|---|---|
| *av* | average |
| *b* | debris bed |
| *c* | cold wall |
| *eff* | effective |
| *max* | maximum value |
| *Na* | sodium |
| *SS* | stainless steel |

temperature of core catcher plate does not exceed 925 K and (ii) sodium trapped inside the debris should not boil, as boiling of sodium is expected to form vapor locking and decrease the effective thermal conductivity of the debris bed and hence ineffective cooling of the debris bed. The present investigation is focused on the fundamentals of heat transfer during turbulent natural convection of sodium with heat source distributed on multiple plates. For this purpose, an ideal enclosure having dimensions close to that of a typical 500 MWe nuclear reactor is considered.

In spite of the importance of natural convection heat transfer in such enclosures in many practical applications, very few basic studies have so far been conducted for enclosures filled with liquid metals. A considerable amount of experimental work was focused on obtaining heat transfer correlations, for natural convection of internally heated fluids, in such geometries. The fluids mostly employed in the experiments were water, mercury and Freon, because of difficulty in handling liquid sodium at the desired experimental conditions. An experimental study of convective heat transfer in liquid-filled vertical annulus of radius ratio, $\lambda = 5.338$ for various aspect ratios has been reported by Prasad and Kulacki [1]. They used water, heptane and ethylene glycol as the test fluids to vary the Prandtl number in the range of 4–196. They found significant curvature effects on the temperature fields and weak dependency of the Nusselt number on the aspect ratio. An extensive study of natural convection in isothermally vertical annuli was reported by de Vahl Davis and Thomas [2]. The key parameters in their analysis were $Ra \leqslant 10^5$, $0.5 < Pr < 10^4$, $1 \leqslant$ aspect ratio (A) $\leqslant 33$ and the radius ratio in the range of 1–4. Their results indicated that the temperature and velocity fields have strong dependency on the radius ratio ($\lambda$) apart from Rayleigh number and aspect ratio. A comprehensive numerical study of natural convection heat transfer of a fluid in vertical annuli with the inner wall maintained at a higher temperature than the outer wall has been carried out by Kumar and Kalam [3]. They reported the results of heat transfer rates and flow fields for $10 \leqslant Ra \leqslant 10^6$, $11 < \lambda < 15$, $0.3 \leqslant$ aspect ratio (A) $\leqslant 10$. An excellent comparison of different numerical and experimental are carried out and discrepancies in the existing numerical and experimental data are noted and discussed. Emara and Kulacki [4] conducted numerical investigations in heat generating fluid layers for the Rayleigh number range of $5 \times 10^3$–$5 \times 10^8$ and the Prandtl number range of 0.05–20, with cooled top wall and adiabatic bottom wall. Ha and Jung [5] carried out a numerical study to investigate three dimensional steady state, conjugate heat transfer of natural convection and conduction in a vertical enclosure housing a heat generating cube. They found a large variation in heat transfer rates from the enclosure walls. Belmonte et al. [6]

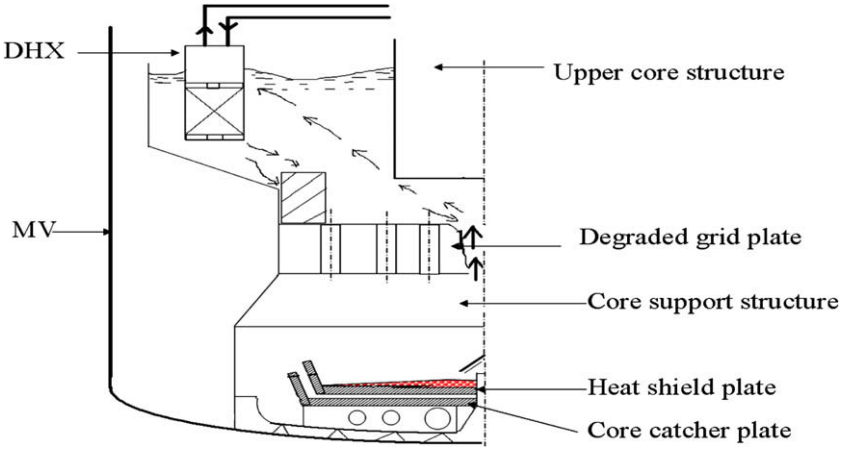


**Fig. 1.** Core catcher housed inside core support structure.

carried out experiments to study the temperature and velocity fields for turbulent Rayleigh–Benard convection in a cubic cell. The experiments were conducted for two different working fluids i.e., water (Pr = 6.6) and air (Pr = 0.7). They measured velocity directly in the case of water, whereas measurement of thermal boundary layer thickness was done in air. They found that for $Ra > 10^7$, the position of the maximum velocity was outside the thermal boundary layer. Conjugate natural convection heat transfer in a two-dimensional, air-filled enclosure of finite conductive walls containing discrete internal heat sources and an internal baffle was examined by Sun and Emery [7]. The influence of the internal heat sources, as well as the conductive baffle, on the heat transfer and the flow characteristics is discussed. The qualitative and quantitative understanding of the influence of conjugate conduction–convection heat exchange and internal–external heating has been presented in this study. A good qualitative agreement has been found between the simulations and measurements. However, the quantitative comparisons showed deviations largely generated due to uncontrollable and dynamic boundary conditions. Zhao et al. [8] developed a conjugate heat transfer model and its solution strategies in enclosures with multiple heat sources. The isotherms, streamlines and Nusselt numbers with wide ranges of external and internal Rayleigh numbers under different thermal boundary conditions were presented to understand the heat transfer characteristics in the enclosure. They concluded that the practice of solving the conjugate heat transfer followed by them performs well, and a sole temperature scale was more flexible than a combined temperature scale for arbitrary strengths of external and internal heat sources.

The detailed literature survey, presented above, indicates that turbulent natural convection of a low Prandtl number fluid within a cylindrical enclosure has not received adequate attention in the open literature. The present study aims at addressing this issue. In this study, turbulent natural convection of sodium is analyzed using numerical solutions of the 2-D axi-symmetric governing equation using a finite volume method. The numerical procedure is validated by simulated experiments carried out in a water model.

## 2. Details of experiments

The basic experimental setup was designed with the core catcher assembly and core support structure having a geometrical similarity with that of reactors. Water is the simulant and the decay heat is simulated with heaters. The system has a maximum capability to produce uniformly distributed heat source of 24 kW in the form of specially designed heaters placed on the heat shield plate. The photograph and dimensional details of the experimental facility are shown in Figs. 2 and 3, respectively. For temperature


**Fig. 2.** Photograph of core catcher experimental facility.

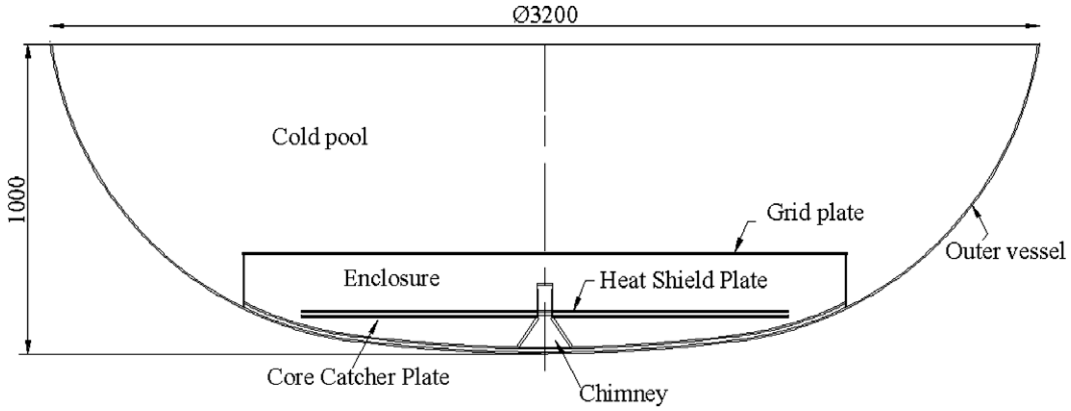


**Fig. 3.** Details of core catcher experimental facility.

mapping of the system, thermocouples were provided at many critical locations and online temperature monitoring was carried out. These thermocouples were S.S. sheathed mineral insulated Chromel–Alumel 'K' type thermocouples with response time ~0.8 s. Since Resistance Temperature Detectors (RTD) are stable and accurate with an accuracy of around 0.3°C, waterproof RTD temperature sensors were placed at 20 places in critical zones such as the inlet and outlet of the chimney and the central axis of the system.

The observed spread in the background temperature with heater power off is 0.14 °C. The system was thermally loaded gradually to the designated power level in stages, with continuous monitoring of heater parameters on the control panel. From room temperature, each steady state was reached in approximately 36 h. For the purpose of calculations and temperature mapping, time average of data for 120 min was taken. Experimental campaigns were conducted for two steady state plate temperatures viz. 318 K and 328 K. The objective of the experiments is to provide data for code validation.

## 3. Numerical analysis

### 3.1. Mathematical formulation

The geometry considered for turbulent natural convection is a 2-D axi-symmetric enclosure shown in as shown in Fig. 4(a–c) for one, two and three plate configurations, respectively. Sodium is assumed to be incompressible. Boussinesq approximation is used to account for the buoyancy force in the vertical momentum equation. The turbulent flow is described mathematically by the Reynolds Averaged Navier Stokes (RANS) equations, including the

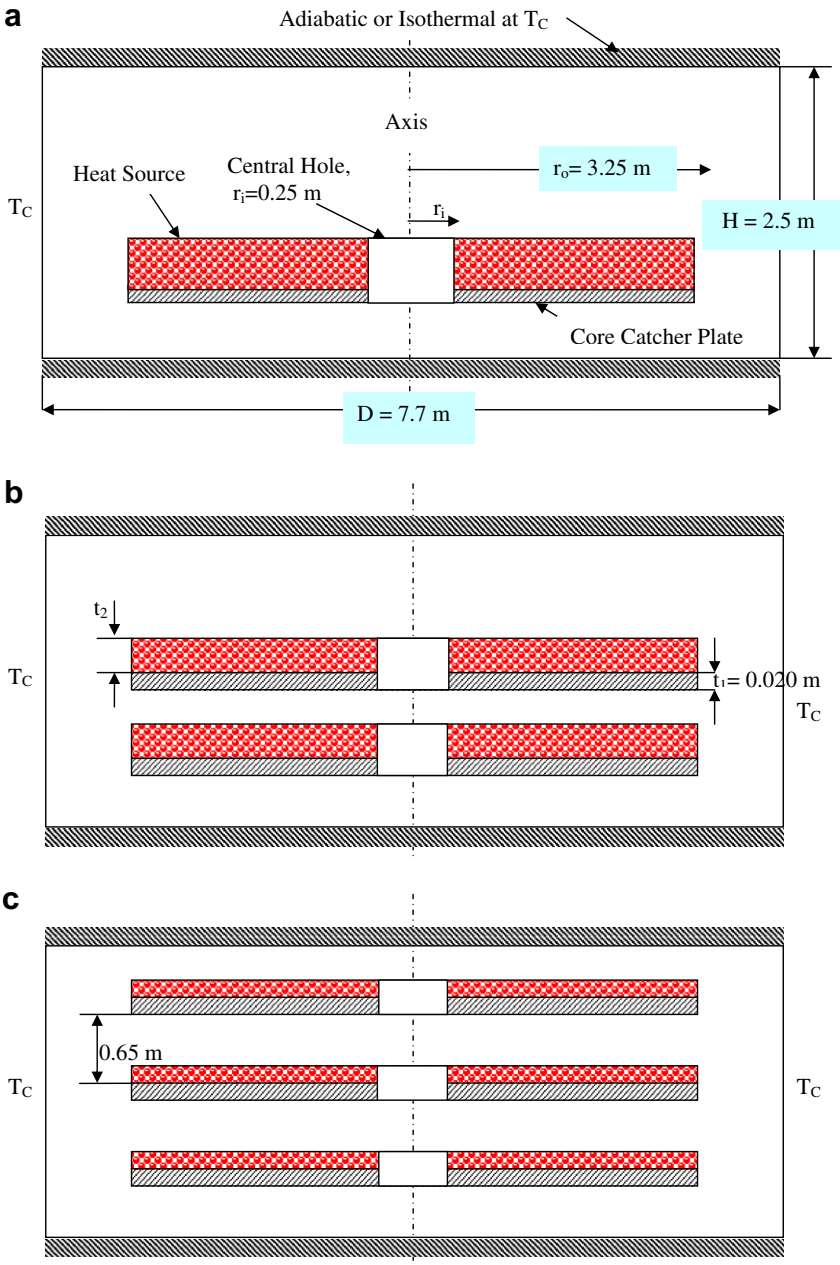


**Fig. 4.** (a) Physical model with the boundary conditions (single plate configuration) (b) Physical model with the boundary conditions (double plate configuration) (c) Physical model with the boundary conditions (triple plate configuration).

time averaged energy equation for the mean temperature field that drives the flow by buoyancy force. Turbulence is modeled by the standard $k$–$\varepsilon$ turbulence closure. The transient form of RANS equations for mass, momentum and energy conservation along with the equation for turbulent kinetic energy ($k$) and its dissipation rate ($\varepsilon$) in sodium are:

(a) Continuity

$$\frac{1}{r}\frac{\partial(ru)}{\partial r}+\frac{\partial(v)}{\partial z}=0 \tag{1}$$

(b) Radial momentum

$$\frac{\partial(\rho_{Na}u)}{\partial t}+\frac{\partial(\rho_{Na}uu)}{\partial r}+\frac{\partial(\rho_{Na}vu)}{\partial z} =-\frac{\partial p}{\partial r}+\frac{1}{r}\frac{\partial}{\partial r}\left(r\mu_{eff}\frac{\partial u}{\partial r}\right)+\frac{\partial}{\partial z}\left(\mu_{eff}\frac{\partial u}{\partial z}\right)-\mu_{eff}\frac{u}{r^2} \tag{2}$$

(c) Vertical momentum

$$\frac{\partial(\rho_{Na}v)}{\partial t}+\frac{\partial(\rho_{Na}uv)}{\partial r}+\frac{\partial(\rho_{Na}vv)}{\partial z} =-\frac{\partial p}{\partial z}+\frac{1}{r}\frac{\partial}{\partial r}\left(r\mu_{eff}\frac{\partial v}{\partial r}\right)+\frac{\partial}{\partial z}\left(\mu_{eff}\frac{\partial v}{\partial z}\right)+g\rho\beta(T-T_{ref}) \tag{3}$$

(d) Energy

$$\frac{\partial(\rho_{Na}C_{Na}T_{Na})}{\partial t}+\frac{\partial(\rho_{Na}C_{Na}uT_{Na})}{\partial r}+\frac{\partial(\rho_{Na}C_{Na}vT_{Na})}{\partial z} =\frac{1}{r}\frac{\partial}{\partial r}\left(rk_{eff}\frac{\partial T_{Na}}{\partial r}\right)+\frac{\partial}{\partial z}\left(k_{eff}\frac{\partial T_{Na}}{\partial z}\right)+q''' \tag{4}$$

(e) Turbulent kinetic energy

$$\frac{\partial(\rho_{Na}k)}{\partial t}+\frac{\partial}{\partial r}(\rho_{Na}uk)+\frac{\partial}{\partial z}(\rho_{Na}vk) =\frac{1}{r}\frac{\partial}{\partial r}\left[r\left(\mu+\frac{\mu_t}{\sigma_k}\right)\frac{\partial k}{\partial r}\right]+\frac{\partial}{\partial z}\left[\left(\mu+\frac{\mu_t}{\sigma_k}\right)\right]\frac{\partial k}{\partial z}+p_k+G_k-\rho\varepsilon \tag{5}$$

(f) Dissipation rate of turbulent kinetic energy

$$\frac{\partial(\rho_{Na}\varepsilon)}{\partial t}+\frac{\partial}{\partial r}(\rho_{Na}u\varepsilon)+\frac{\partial}{\partial z}(\rho_{Na}v\varepsilon) =\frac{1}{r}\frac{\partial}{\partial r}\left[r\left(\mu+\frac{\mu_t}{\sigma_\varepsilon}\right)\frac{\partial\varepsilon}{\partial r}\right]+\frac{\partial}{\partial z}\left[\left(\mu+\frac{\mu_t}{\sigma_\varepsilon}\right)\right]\frac{\partial\varepsilon}{\partial z} +[C_{\varepsilon1}(P_k+C_{\varepsilon3}G_k)-C_{\varepsilon2}\varepsilon]\frac{\varepsilon}{k} \tag{6}$$

$$P_k=\mu_t\left[2\left(\frac{\partial u}{\partial r}\right)^2+2\left(\frac{\partial v}{\partial z}\right)^2+\left(\frac{\partial u}{\partial z}+\frac{\partial v}{\partial r}\right)^2+2\left(\frac{u}{r}\right)^2\right];$$

$$G_k=-\frac{\mu_t}{\sigma_T}g\beta\frac{\partial T_{Na}}{\partial r};\quad \mu_{eff}=\mu+\mu_t;$$

$$\mu_t=C_\mu\frac{\rho k^2}{\varepsilon}\quad\text{and}\quad K_{eff}=K+\frac{\mu_t c_p}{\sigma_T}.$$

For k-ε turbulence model, the following constants are used $C_\mu = 0.09$; $C_{\varepsilon1} = 1.44$; $C_{\varepsilon2} = 1.92$; $\sigma_T = 0.9$; $\sigma_K = 1.0$ and $\sigma_\varepsilon = 1.3$

The value of, $C_{\varepsilon3}$ is taken as tanh $(u/v)$, as suggested by Henkes [9]. No wall functions are used and sufficiently fine grids are employed close to the walls to enable integration up to the walls.

Conduction is the mode of heat transfer within the debris and the temperature distribution in the core debris bed is governed as follows:

$$\frac{\partial(\rho_b C_{pb}T_b)}{\partial t}=\frac{1}{r}\frac{\partial}{\partial r}\left(rk_b\frac{\partial T_b}{\partial r}\right)+\frac{\partial}{\partial z}\left(k_b\frac{\partial T_b}{\partial z}\right)+q''' \tag{7}$$

The thermo-physical properties of austenitic stainless steel, liquid sodium and debris at operating temperature range used in the simulations are given in Table 1. The debris bed is a homogeneous mixture of sodium and solid particles (fuel and steel). The porosity of the bed ($\phi$) is assumed to be 0.4. The effective thermal conductivity of the bed ($k_b$) is calculated based on the Kampf and Karsten formula as given below [10].

$$K_b=K_{Na}\left[1-\frac{(1-\phi)\left(1-\frac{K_p}{k_{Na}}\right)}{\frac{K_p}{K_{Na}}+(1-\phi)^{1/3}\left(1-\frac{K_p}{K_{Na}}\right)}\right] \tag{8}$$

where $K_{Na}$ is the effective thermal conductivity of sodium, $K_p$ is effective thermal conductivity of the solid particles given by $\frac{1}{K_p}=\sum\frac{\alpha_i}{K_i}$ and $\alpha_i$ is mass fraction of component with conductivity of $K_i$ and the specific heat of bed is calculated as $c_{pb}=\sum\alpha_i c_{p_i}$, where $c_{pi}$ is the specific heat of the component $i$.

The temperature distribution in the stainless steel core catcher plates/trays is governed by

$$\frac{\partial(\rho_{ss}C_{ss}T_{ss})}{\partial t}=\frac{1}{r}\frac{\partial}{\partial r}\left(rk_{ss}\frac{\partial T_{ss}}{\partial r}\right)+\frac{\partial}{\partial z}\left(k_{ss}\frac{\partial T_{ss}}{\partial z}\right) \tag{9}$$

Along the sodium-debris, sodium steel and debris steel interfaces, temperature and heat flux are continuous.

### 3.2. Initial and boundary conditions

The physical dimensions of the enclosure are marked in Fig. 4a. The diameter of core catcher plate is 6.5 m and its thickness of 20 mm. The diameter ($D$) and the height ($H$) of the cylindrical enclosure are 7.7 m and 2.5 m, respectively. An axial gap of 0.580 m is maintained between the bottom of core catcher plate and the enclosure bottom. A central hole of diameter 0.5 m is provided to facilitate natural convection. In the case of multiplate core catcher concepts, the core catcher plates are staged at an axial pitch of 650 mm. The total volume of the core debris is 5.12 m$^3$ assumed to be distributed uniformly. The ideal assumption of uniform spread of core debris is more close to realty, as the bed formed is normally a shallow cone. When the heap formed is a high cone it eventually tapers off due to sodium boiling. The Boussinesq number based on volumetric heat generation rate, q$'''$ enclosure dimensions and sodium properties varies in the range of $4.5\times10^{11}$–$6.25\times10^{12}$.

The lateral surface of cylinder is considered as isothermal at ($T_c$ = 673 K). This corresponds to the typical temperature of the cold pool in which the enclosure is submerged. The bottom and the top walls of the enclosure are adiabatic. Symmetry boundary conditions are imposed on the vertical axis (i.e., at $r = 0$, $u = 0$ and

**Table 1**
Thermo-physical properties of austenitic stainless steel, liquid sodium and debris bed at operating temperature range.

| Properties | Stainless steel | Debris bed | Liquid sodium |
|---|---|---|---|
| Density ($\rho$), kg/m$^3$ | 8029.5 | 6293.6 | 849.9 |
| Specific heat ($C_p$), J/kg K | 502.5 | 964.5 | 1272.6 |
| Thermal conductivity ($K$),W/m K | 16.3 | 23.8 | 69.7 |
| Isobaric cubical expansion coefficient of fluid ($\beta$), K$^{-1}$ | – | – | $2.8\times10^{-4}$ |
| Kinematic viscosity of fluid ($v$), m$^2$/s | – | – | $3.15\times10^{-7}$ |

radial derivatives of $T$, $v$, k and ε are set to zero). No slip boundary conditions are used for the entire solid- fluid interface i.e. $u = 0$, $v = 0$ and $k = 0$ and $\varepsilon = \infty$. The value of '$\varepsilon$', is set to $10^{25}$ on the walls for numerical implementation purpose and its sensitivity on the predicted heat transfer results is examined. It is varied from $10^5$ to $10^{30}$ and found that the results remain insensitive to its numerical value greater than $10^{20}$. Hence, in the present study the numerical value of '$\varepsilon$' is set to $10^{25}$ at walls. The debris constitutes a uniform volumetric heat source. In one of the parametric studies, the top surface of the enclosure is also kept isothermal at $T_c$. Sodium is initially assumed to be stagnant at $T_c$.

### 3.3. Numerical procedure

For the numerical solution of the governing equations, the primitive variable approach is adopted. The spatial derivatives in the equations are discretized using the finite-volume method. The governing equations are integrated over the control volume surrounding a grid point. A first order upwind scheme is employed to estimate the flux on the control volume surfaces. Since there is a large variation in thermal conductivity between the sodium, the core catcher plate and the core debris harmonic interpolation is used to estimate interface conductivity values in the conjugate heat transfer simulations. Non uniform size staggered grids are used that give adequate grid refinement close to the solid surfaces. SIMPLE algorithm proposed by Patankar and Spalding [11] is used to resolve pressure- velocity coupling. The discretised equations are solved by the line by line Thomas algorithm, using two directional sweeps. A fully implicit method has been used for the time integration. At any time step, the solution is considered to be converged when the normalized absolute sum of the residuals in the discretisation equations are reduced by at least three orders of magnitude. The time step, $\Delta t$, is chosen from time step independence studies. It is found that a time step of 0.2 s is optimum to reach steady state.

### 3.4. Grid-independence study

A thorough grid-independence check of the numerical solutions was carried out. For the single plate analysis, the number of grid points used is 200 × 100 in the radial and axial directions. Fig. 5 shows the predicted variation of non-dimensional temper-

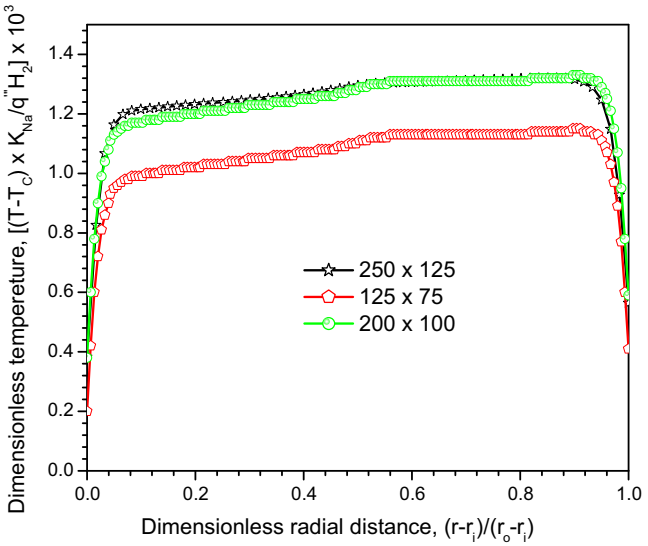


**Fig. 5.** Grid dependence tests of the solution: Non- dimensional temperature variation on the top of core catcher plate for heat generation rate, $q''' = 5.0 \times 10^5$ W/m$^3$.

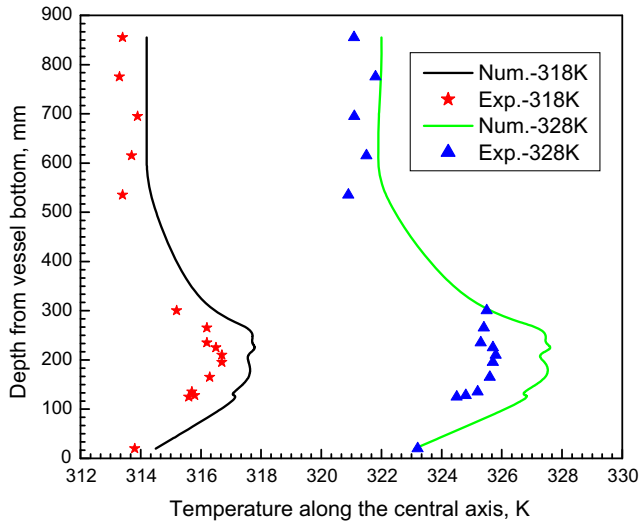


**Fig. 6.** Comparison of numerical and experimental results for a steady state temperature of heat shield plate at 318 K and 328 K.

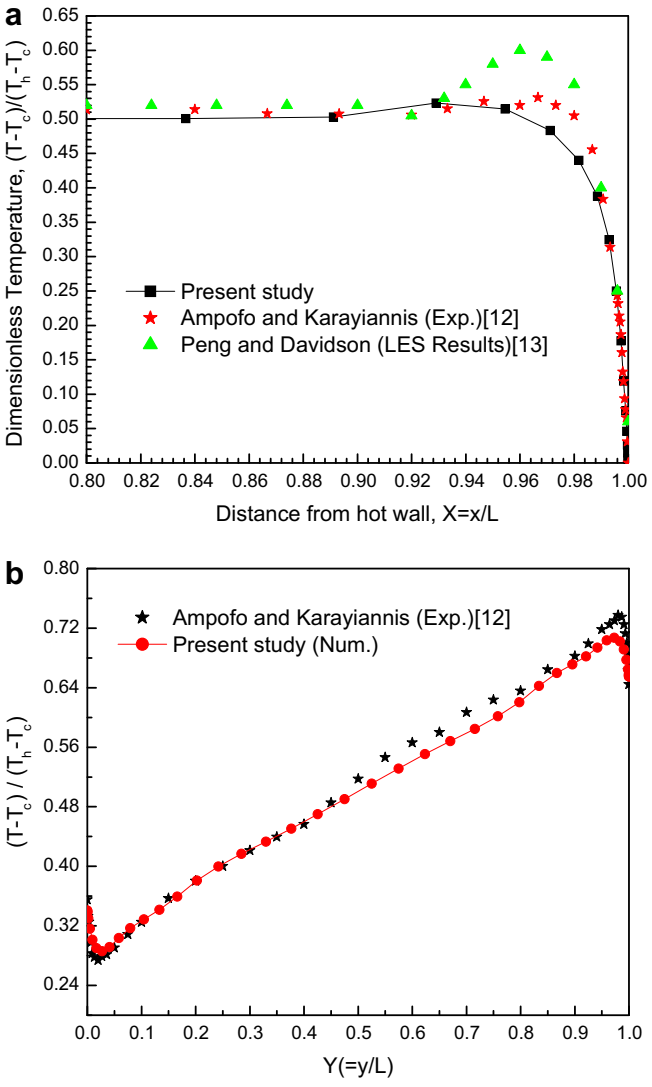


**Fig. 7.** Comparison of mean temperature distribution along (a) Mid height and (b) Mid width.

ature on the core catcher plate as a function of the non-dimensional radius for a specific heat generation rate of $5 \times 10^5$ W/m$^3$ for three different grid patterns of $125 \times 75$, $200 \times 100$ and $250 \times 125$. It is clear that the grid pattern of $200 \times 100$ is fine enough to produce grid independent solutions. The maximum difference in Nusselt number on the lateral surface of the enclosure for various grids is found to be less than 0.75%, indicating that a $200 \times 100$ grid is sufficient to model the heat transfer and fluid flow inside the enclosure. Hence, a grid $200 \times 100$ has been used in all the subsequent computations. Similar grid independence tests for other two geometries were also carried out.

### 3.5. Validation of numerical results with experimental data

Numerically predicted temperature distribution along the centerline of the experimental model is compared against the measured values in Fig. 6 for two different steady state temperatures of the plate viz. 318 K and 328 K, respectively. It can be seen that the comparison is satisfactory with the computational model marginally over predicting the temperature of the pool, conservatively.

### 3.6. Validation of numerical results with benchmark solutions

Due to lack of standard results for cylindrical enclosures, the turbulence model used in the present code is validated against, the experimental benchmark data of Ampofo and Karayiannis [12]. These authors have conducted an experimental study of turbulent natural convection in an air-filled vertical square enclosure of 0.75 m high $\times$ 0.75 m wide $\times$ 1.5 m deep giving a two-dimensional flow in middle plane. The vertical hot and cold walls are isothermal at 50 °C and 10 °C, respectively, giving a Rayleigh number of $1.58 \times 10^9$. A comparison of the mean temperature distribution along the mid-height and the mid-width is shown in Fig. 7(a) and (b) along with the LES results of Peng and Davidson [13]. As seen in the figure, the agreement among the present numerical, experimental and the LES results is satisfactory. The present numerical method was further validated against the benchmark numerical simulations of Henkes and Hoogendoorn [14] and Ridouane et al. [15]. Fig. 8 compares the solution obtained in the present study against the published solution for Rayleigh number = $5 \times 10^{10}$. Due to the large value of the Rayleigh number, thin boundary layers have formed along the vertical walls and the turbulence is confined to a part of the vertical boundary layers.

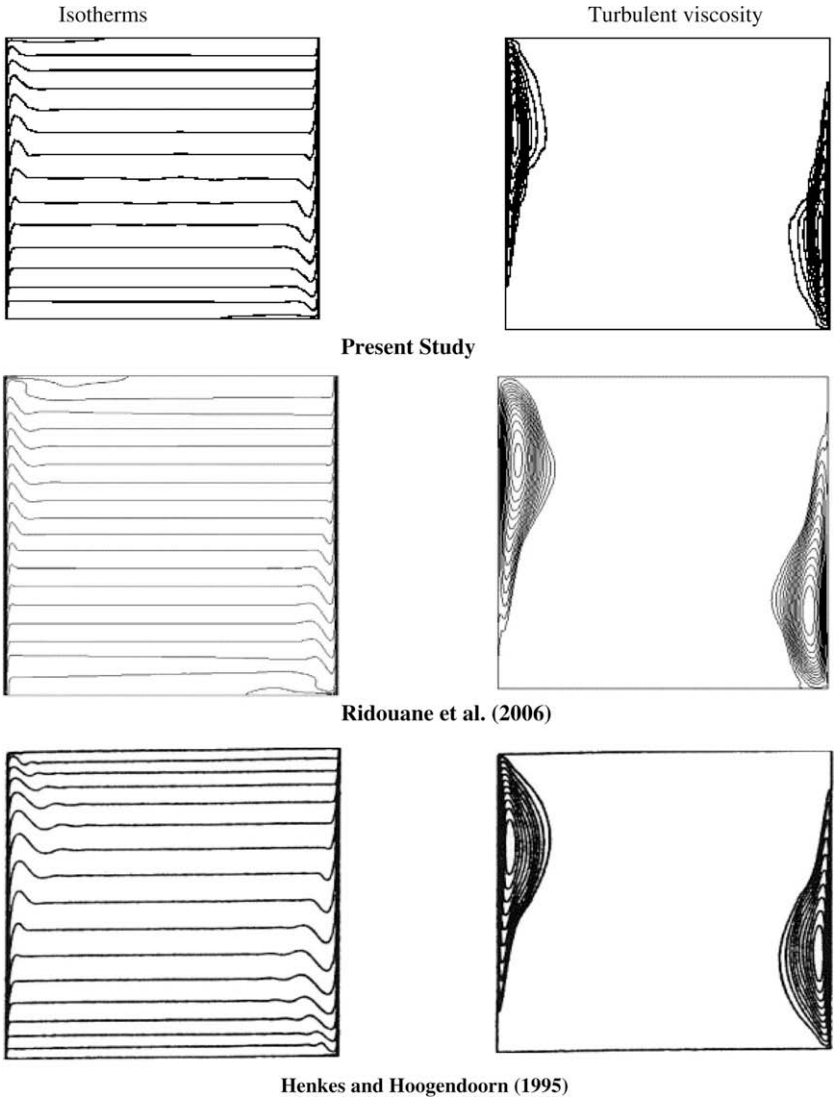


**Fig. 8.** Comparison of temperature field and turbulent viscosity for a square cavity at Ra = $5 \times 10^{10}$ against the results of Ridouane et al. [15] and Henkes and Hoogendoorn [14].

These validation studies demonstrate that the code developed is capable of predicting natural convection in enclosure for stable and unstable stratification regimes.

## 4. Results and discussion

As mentioned earlier, the focus of this paper is fluid flow and heat transfer from single and multiple volumetric heat sources with a special concern on maximum temperature in the plates and temperature field inside the liquid sodium pool. Steady state is achieved by solving the transient forms of governing equations. Steady state is assumed to be reached when the heat imbalance between the heat source and the heat sink is $\leqslant 0.1\%$.

### 4.1. Single plate configuration

A detailed parametric study has been carried out for various values of volumetric heat generation rates ($q'''$), varying from 0.5 MW/m$^3$ to 3.0 MW/m$^3$ in the debris bed placed over the single core catcher plate (single collection tray). Steady state isotherms predicted for three different values of $q'''$ are shown in Fig. 9(a)–(c) and the corresponding streamlines are depicted in Fig. 10(a)–(c). The heat generated in the source is dissipated by conduction and natural convection to the lateral wall of the enclosure. At low heat generation rates, the heat penetrates through the fluid and dissipates predominantly by conduction because of high thermal diffusivity of sodium. However, as the heat generation rate increases, the convection contribution increases. There is a strong downward flow along the cold side wall. The flow is radially outward along the top wall and inward along the bottom wall. Around the core catcher plate the flow is outward at its bottom and inwards at its top. The streamlines are closely packed around side and top walls of the enclosure indicating strong velocity gradients and boundary layer flows. Sparsely spared streamlines on the top of core debris suggest lower horizontal velocities due to unstable stratification (bottom sodium layer hotter than the top layer). The radial gap between the sidewall and the core catcher plate is large to accommodate both the upward and downward legs of natural convection flow. There is a flow separation zone at the periphery of the core catcher plate. The fraction of flow through the central hole is not significant. However, there is flow through the central hole. It can be seen in Fig. 10(b) that there are two mild separation bubbles on the top of the core debris. The first bubble is due to flow separation induced by the horizontal debris bed. When the cold fluid gets heated after the reattachment point, it tries to rise up due to favorable buoyancy thus leading to the formation of the second bubble. There is a strong correlation between the stream lines and isotherms depicted in Figs. 10(b) and 9(b), respectively. The magnitude of the fluid motion depends on the strength of the source, which determines the temperature gradient that drives the natural convective. Accordingly, the magnitude of the streamlines (the measure of the natural convective flow rate within the enclosure) is seen to increase as $(q''')^{0.5}$. This is expected because in natural convection, typically the velocity is proportional to $\Delta T^{0.5}$ and $\Delta T$ is proportional to $q'''$.

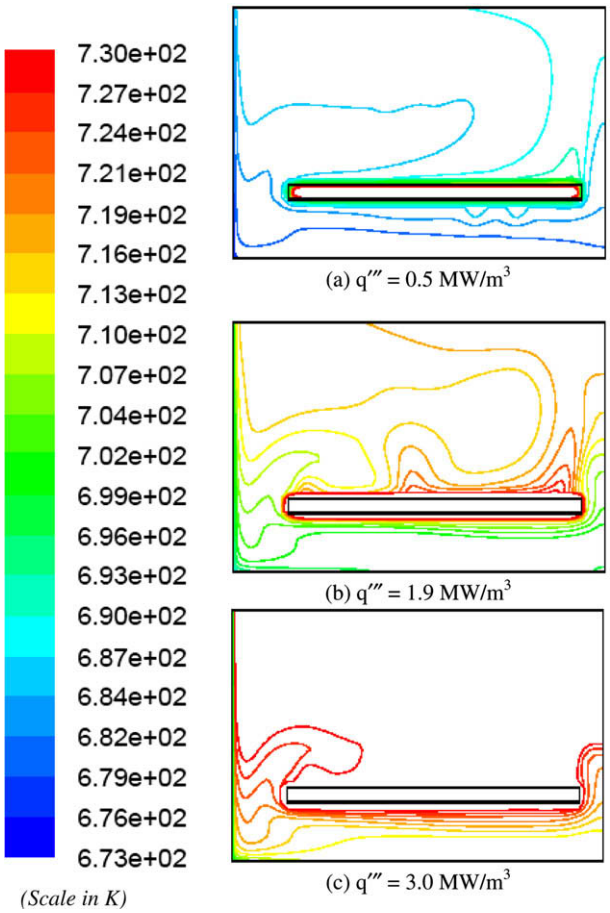


**Fig. 9.** Isotherms in the enclosure for various values of volumetric heat generation rates.

Fig. 11 shows the temperature distribution in the core catcher plate along the radial direction for various values of heat generation rates. With $q'''$ as 0.5 MW/m$^3$, it is clear that the temperature of the core catcher plate is 725 K with the bulk sodium temperature in the enclosure 685 K and the maximum temperature in the debris 765 K. This situation corresponds to a total heat load of 2.2 MW on the core catcher plate. For the case of $q''' = 2.2$ MW/m$^3$, the bulk fluid temperature is 710 K and the maximum temperature in the debris is 1080 K. The core catcher plate temperature is 925 K. This corresponds to a total heat load of 9.5 MW on the core catcher. Therefore, a heat load of 9.5 MW can be easily accommodated by respecting the design limits ($T_{CCP} < 925$ K and $T_{debris\ bed} < 1173$ K). It may be highlighted that for typical 500 MWe fast reactor core, the decay power is $\sim$25 MW$_t$. Thus, there is a need to explore the possibility of distributing the heat source in multiple plates.

### 4.2. Influence of top wall boundary condition on fluid flow and heat transfer characteristics

In Section 4.1, the top wall of the enclosure was assumed to be adiabatic. But it is essential to assess the effects of additional cooling from the top wall on the temperature distribution in the core catcher and its heat dissipation capacity. With this objective, the top wall is also assumed to be isothermal at 673 K in addition to the side wall.

Figs. 12(a) and (b) show the isotherms in the enclosure at a specific heat generation rate of $q''' = 3.0$ MW/m$^3$ without and with top wall cooling. It is clear that there is marked change in the temperature field above the core catcher plate and approximately 64% of total heat transfer is through the top wall. With the addition of top wall cooling, the flow distribution above the debris is well defined with a large size single convection loop engulping the core debris and the core catcher plate. Fig. 13 gives the variation of core catcher plate temperature for different heat generation rates. The plate temperature is lower than that discussed in Section 4.1. But the reduction, however, is not much. The maximum temperature in the debris bed ($T_{max}$) and the bulk sodium temperature ($T_{av}$) in the enclosure are also less when the top wall is also cooled as can be seen in Fig. 14. This indicates that the critical temperatures

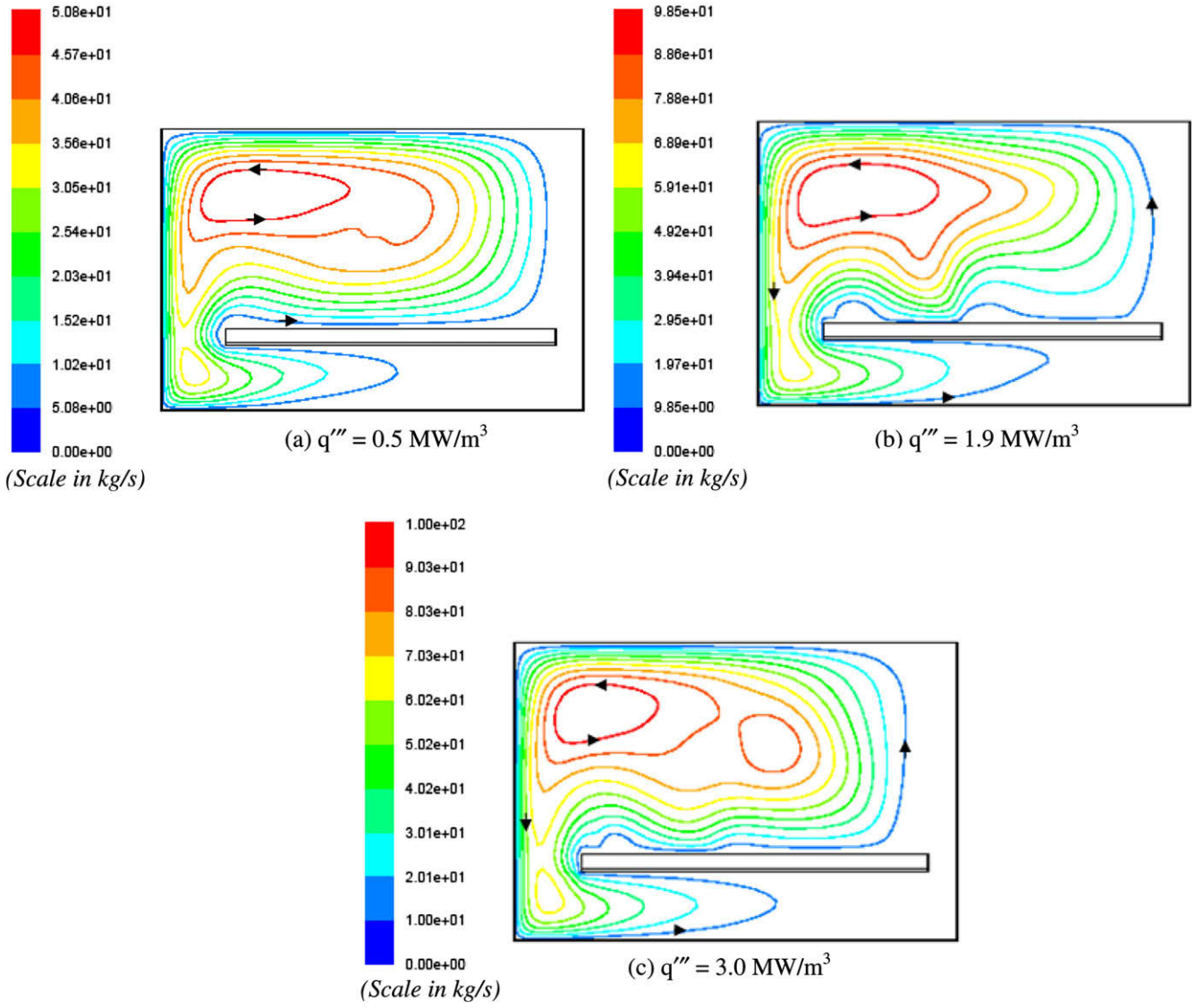


**Fig. 10.** Stream function in the enclosure for various values of volumetric heat generation rates.

are governed by the surface area of the heat source, rather than surface area of the heat sink (top and lateral walls).

### 4.3. Double plate configuration

As the capacity of the single core catcher plate is limited to ~9.5 MW, the capacity of double plate core catcher needs to be investigated. In this, the core debris is engineered to settle on two plates placed one over the other, without increasing the size of the enclosure. The physical model of the double plate arrangement is depicted in Fig. 4(b). Isotherms and stream functions in the enclosure for this configuration for two extreme values of $q'''$ are depicted in Figs. 15 and 16, respectively. It is seen that the flow rate through the central hole increases as we move from the bottom plate to the top plate. This augmentation is due to the inter-plate flow traveling towards the centre. There appears to be only one major recirculation that covers both the trays. The inter-plate flow cools both the top plate and debris in the bottom plate. Also, the debris bed height is less, as the debris volume is distributed to two plates. Due to these reasons, the core catcher plate temperature is much lower than that in the single plate case for the same heat load. For example, in the case of heat generation rate of 3 MW/m$^3$, the

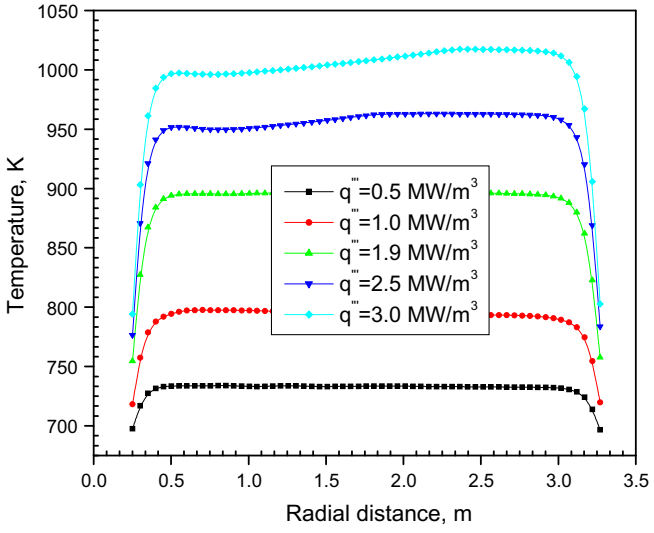


**Fig. 11.** Steady-state temperature on the top of the core catcher plate for different values of heat generation rate in the debris.

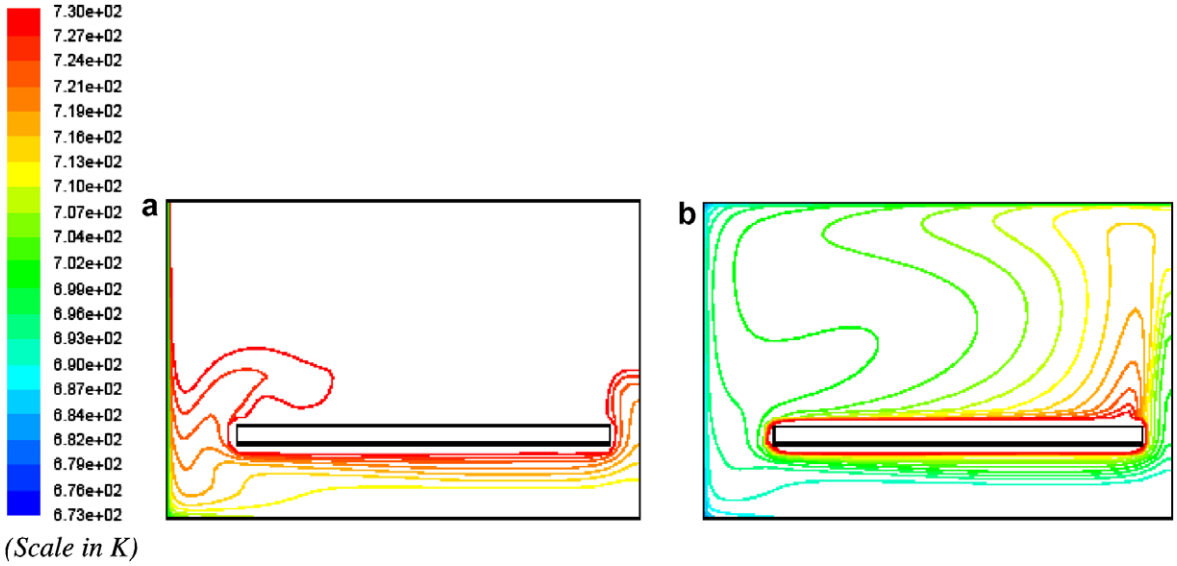


**Fig. 12.** Isotherms in the enclosure for $q''' = 3.0\ MW/m^3$: (a) Top wall adiabatic and side wall isothermal and (b) Top and side wall isothermal at $T_C$.

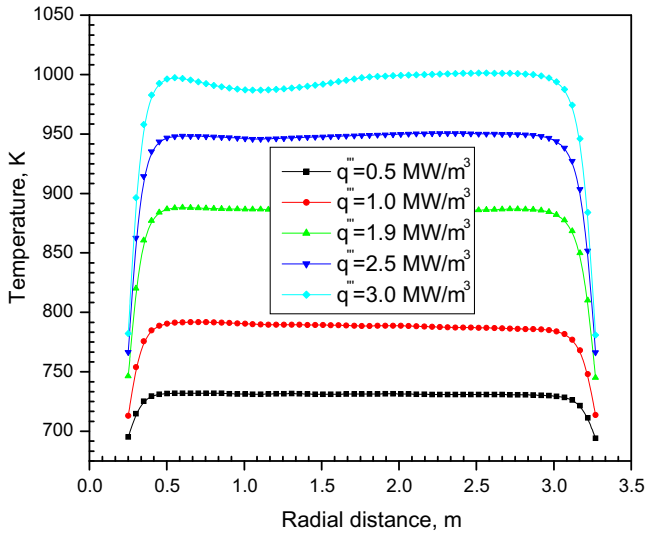


**Fig. 13.** Steady-state temperature in core catcher plate when both the top and side wall are isothermal.

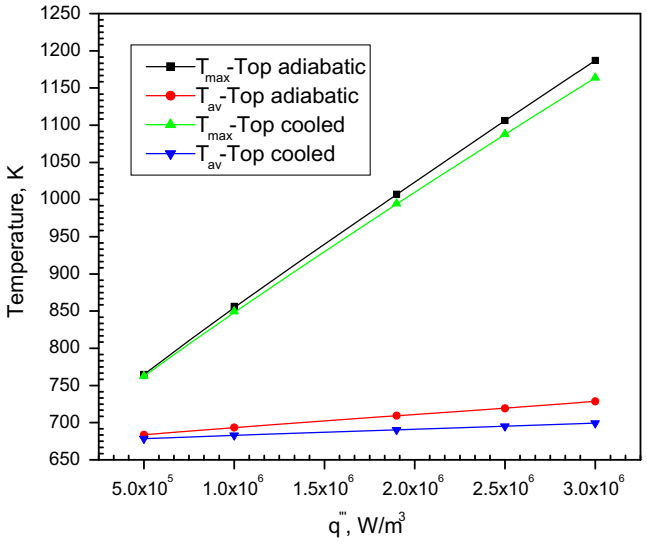


**Fig. 14.** Maximum temperature in the core debris and bulk sodium temperature for different heat generation rates in debris for two different boundary conditions.

maximum plate temperature in the double plate arrangement is 840 K against 1020 K in the case of the single plate arrangement. It is seen from the magnitude of the stream function that the recirculation is nearly same as that of the single plate arrangement.

The temperature of the upper plate is always higher than that of the lower plate, as can be seen in Fig. 17. This is because the upper debris bed is washed by partially heated recirculating sodium while the bottom debris is washed by completely cooled sodium. For the case of $q''' = 4.6\ MW/m^3$ the temperatures of the upper and lower plate are 920 K and 880 K, respectively, which are acceptable. This corresponds to a total power of 20 MW and hence a heat load of 20 MW can be dissipated by respecting the temperature limits. This is nearly double the value seen in the single plate arrangement.

### 4.4. Triple plate configuration

In order to assess if the heat load capacity increases further, a triple plate arrangement is studied. The physical model of the three plate configuration is depicted in Fig. 4(c). The predicted temperature and stream function distributions are presented in Figs. 18 and 19, respectively for the triple plate arrangement, for two different heat generation rates. There is a flow separation at the periphery of all the plates. The natural convection flow is predominantly to outwards at the bottom and inwards at the top of all the core catcher plates. The magnitude of velocity in the present arrangement was nearly the same as seen in the case of double plate configuration for identical heat generation rates. For example, in the case of $q''' = 7.0\ MW/m^3$, the maximum velocity was found to be 0.34 m/s as compared to the value of 0.41 m/s in the two plate configuration.

The temperature distribution in the plates for triple plate arrangement is depicted in Fig. 20. Temperatures of the upper, middle and lower plate are found to be 922 K, 900 K and 865 K, respectively, for a heat generation rate of $q''' = 5.76\ MW/m^3$ that corresponds to 25 MW load. The maximum temperature in the debris bed for this load is 949 K, which is also less than sodium boiling limit. These values are acceptable and hence, a triple tray concept can dissipate a heat load of 25 MW.

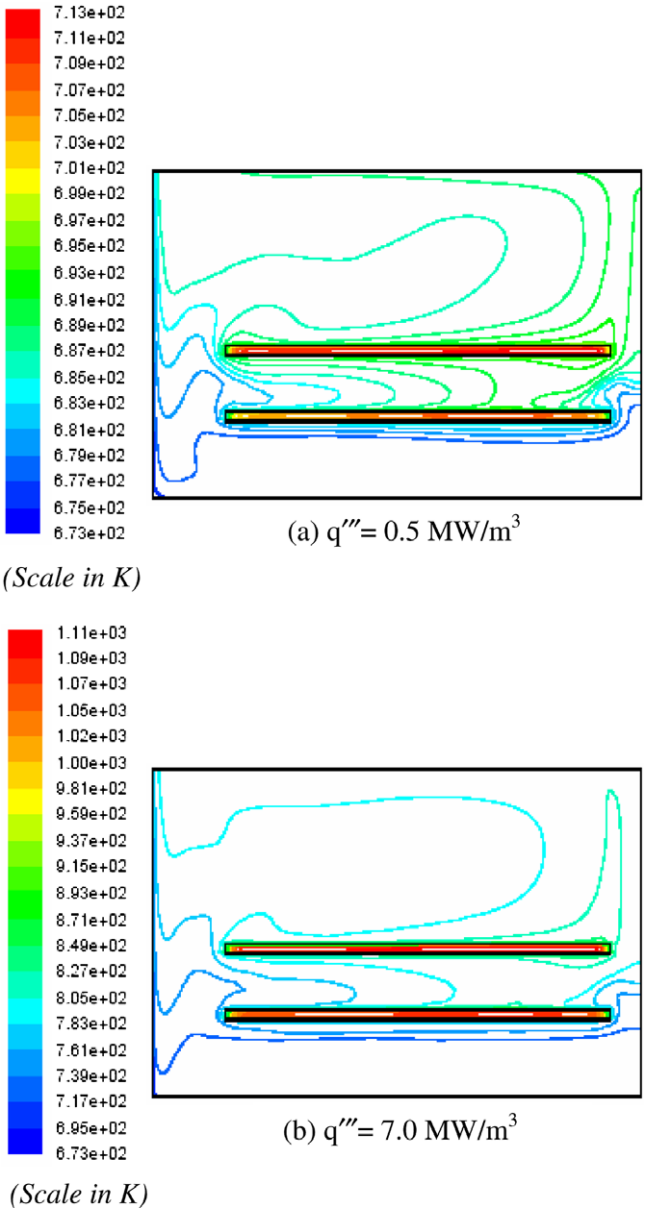


**Fig. 15.** Isotherms in the enclosure for double plate arrangement.

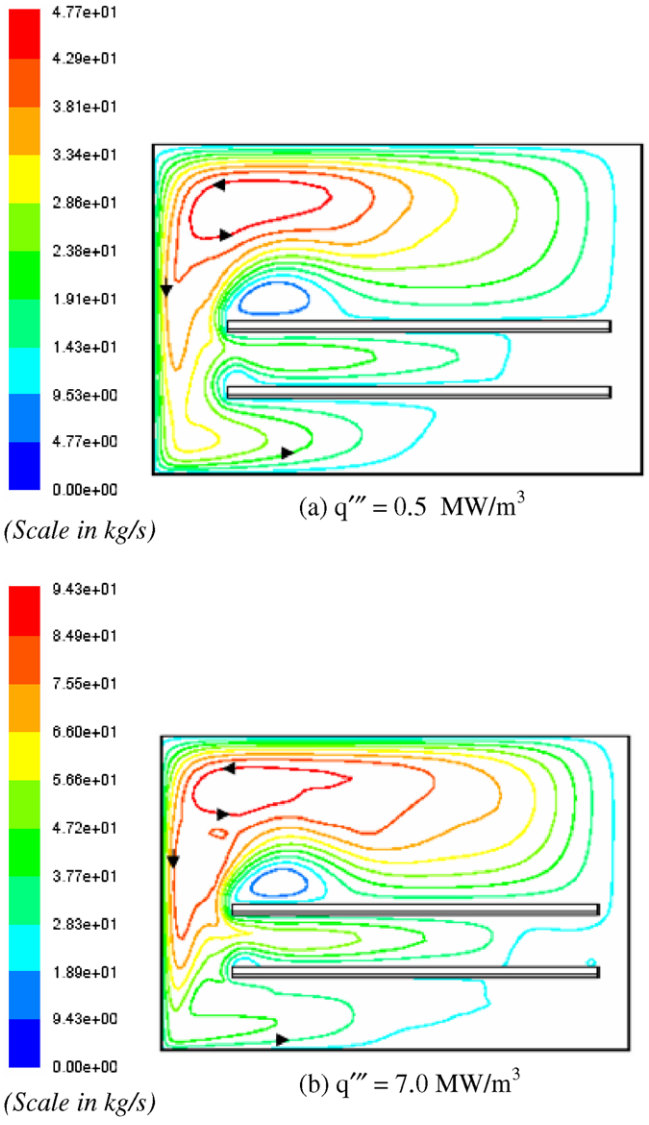


**Fig. 16.** Stream function in the enclosure for double plate arrangement.

Fig. 21 shows the maximum temperature in the core debris with heat generation rate. For example, at a heat generation rate of $q''' = 3.0\ MW/m^3$, the maximum temperatures in the debris for the case of singe, double and triple plates configurations are 1187 K, 873 K and 826 K, respectively. It is also clear from this figure, that the case of $q''' = 7.0\ MW/m^3$, which corresponds to the total heat load on core catcher of 30 MW, the maximum temperatures in the debris reached are 1112 K and 1001 K for the two and three plate concepts, respectively, which are below the sodium boiling point at that location. Comparing the heat dissipation capacities of single, double and triple plate arrangements, it is clear that the heat dissipation capacity in a non-linear function of the number of plates.

## 5. Conclusions

Turbulent natural convection of liquid sodium in a cylindrical enclosure with distributed heat sources has been investigated for the Boussinesq number in the range of $4.5 \times 10^{11}$–$6.25 \times 10^{12}$. Detailed parametric studies have been carried out with the heat source distributed in single and multiple plates to assess the dissipation

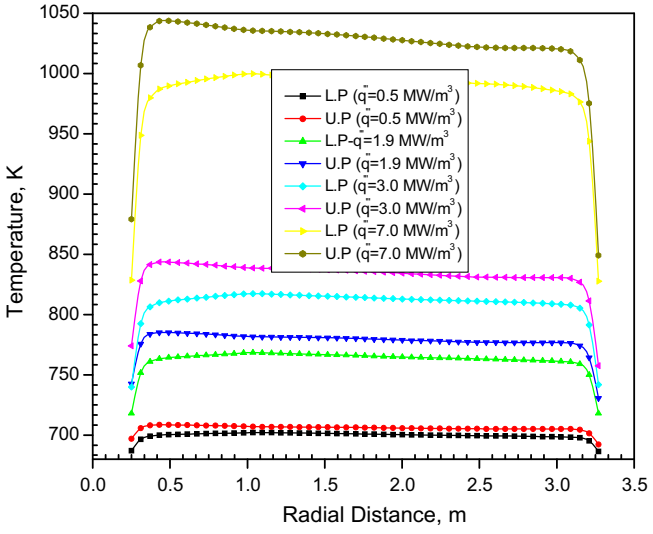


**Fig. 17.** Temperature distribution in the upper (U.P.) and Lower (L.P.) plates.

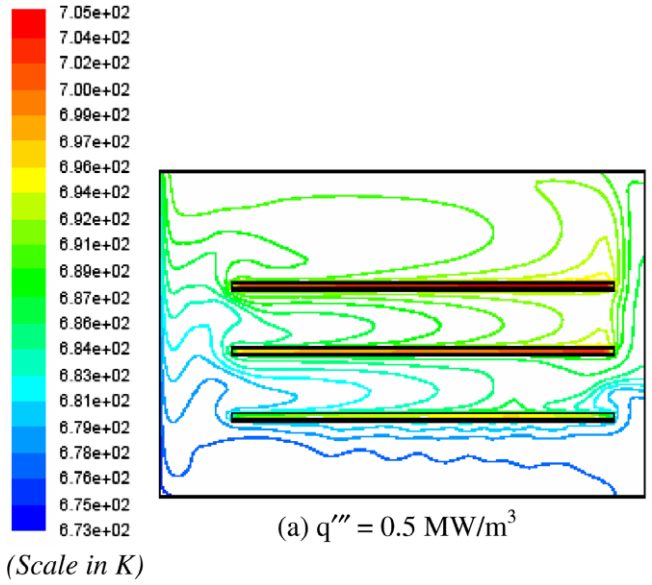


**Fig. 18.** Isotherms in the enclosure for the triple plate configuration.

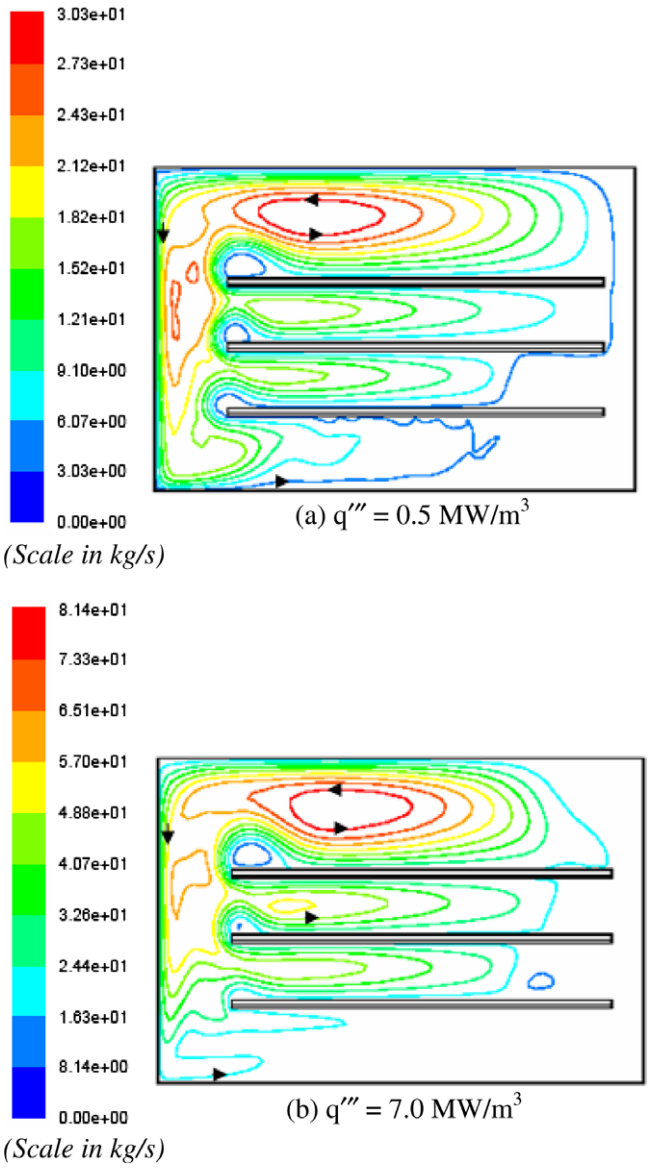


**Fig. 19.** Stream functions in the enclosure for the triple plate configuration.

capacity of different arrangements without exceeding two specific temperature limits, viz. plate temperature <925 K and sodium temperature within the heat sources is <1173 K. The equations that govern turbulent natural convection have been solved numerically by a finite volume method along with heat conduction equation for the debris bed and steel plates. Experiments have been conducted in water on a geometrically similar model towards validating the computational model.

The major conclusions from the numerical investigations are:

(i) With the single and double plate arrangements, heat transfer is limited by the source area. This is evident from linear dependence of heat removal capacity with the number of plates. However, when the number of plates increases further, the heat removal appears to be controlled by the sink area (i.e., side wall).
(ii) With the single plate, the admissible Boussinesq number is $1.9 \times 10^{12}$ and corresponding heat dissipation rate is 9.5 MW.
(iii) When the heat load is distributed in the two plates, the admissible Grashof number is $4 \times 10^{12}$ and the total heat

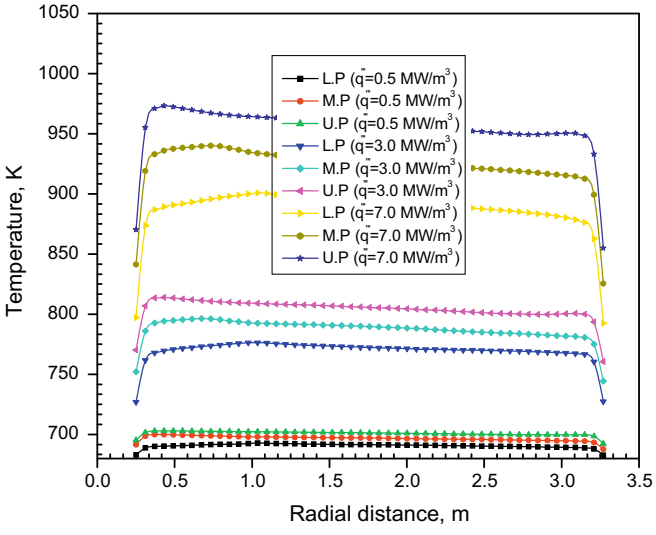


**Fig. 20.** Temperature distribution in the upper (U.P.), middle (M.P.) and Lower (L.P.) plates.

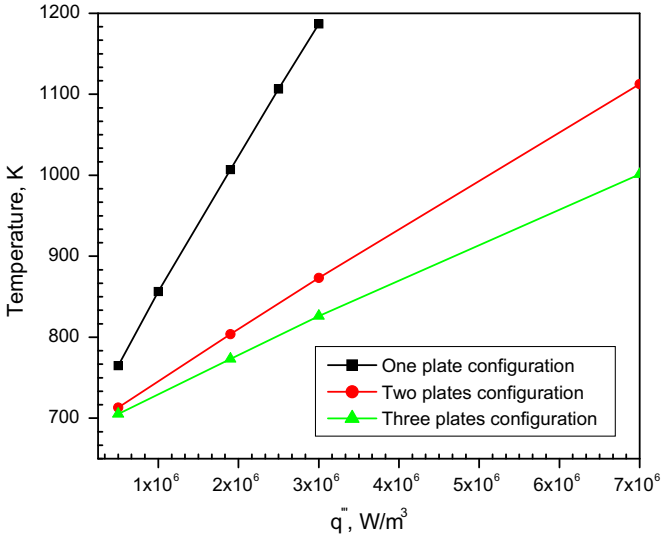


**Fig. 21.** Maximum temperature in the core debris for different heat generation rates in debris for different plate configuration.

dissipation rate is 20 MW. The corresponding values with triple plate arrangement are $5.0 \times 10^{12}$ and 25 MW.

(iv) When the top wall of the enclosure is also cooled, in addition to the side wall, there are marked changes in the flow and temperature distributions, with ~64% of total heat transfer through the top plate. However, the changes in the plate temperature and maximum temperature of sodium source in the source are only marginal (~25 K), for the single plate arrangement.

## References

[1] V. Prasad, F.A. Kulacki, Free convective heat transfer in a liquid-filled vertical annulus, ASME J. Heat Transfer 107 (1985) 596–602.
[2] G. deVahl Davis, R.W. Thomas, Natural convection between concentric vertical cylinders high speed computing in fluid dynamics, Phys. Fluids 5 (1969) 198–207 (Suppl. II).
[3] R. Kumar, M.A. Kalam, Laminar thermal convection between vertical coaxial isothermal cylinders, Int. J. Heat Mass Transfer 34 (1991) 513–524.
[4] A.A. Emara, F.A. Kulacki, A numerical investigation of thermal convection in heat generating fluid Layers, ASME J. Heat Transfer 102 (1980) 531–537.
[5] M.Y. Ha, M.J. Jung, A numerical study of three dimensional conjugate heat transfer of natural convection and conduction in a differentially heated cubical enclosure with a cubic heat generating body, Int. J. Heat Mass Transfer 43 (2000) 4229–4248.
[6] A. Belmonte, A. Tilgner, A. Libchaber, Temperature and velocity boundary layers in turbulent convection, Phys. Rev. E 50 (1994) 269–282.
[7] Y.S. Sun, A.F. Emery, Effects of wall conduction internal heat sources and an internal baffle on natural convection heat transfer in a rectangular enclosure, Int. J. Heat Mass Transfer 40 (1997) 915–929.
[8] Fu-Yun Zhao, Guang-Fa Tang, Di Liu, Conjugate natural convection in enclosures with external and internal heat sources, Int. J. Eng. Sci. 44 (2006) 148–165.
[9] R.A.W.M. Henkes, Natural Convection Boundary Layers, Ph.D. thesis, Delft University of Technology, The Netherlands, 1990.
[10] H. Kampf, G. Karsten, Effects of different types of void volumes on the radial temperature distribution of fuel pins, Nucl. Appl. Technol. 9 (1970) 288–300.
[11] S.V. Patankar, D.B. Spalding, A calculation procedure for heat mass and momentum transfer in three dimensional parabolic flows, Int. J. Heat Mass Transfer 15 (1972) 1787–1806.
[12] F. Ampofo, T.G. Karayiannis, Experimental bench mark data for turbulent natural convection in an air filled square cavity, Int. J. Heat Mass Transfer 46 (2003) 3551–3572.
[13] S.H. Peng, L. Davidson, Large eddy simulation for turbulent buoyant flow in a confined cavity, Int. J. Heat Fluid Flow 22 (2001) 323–331.
[14] R.A.W.M. Henkes, C.J. Hoogendoorn, Comparison exercise for computations of turbulent natural convection in enclosures, Num. Heat Transfer B 28 (1995) 59–78.
[15] E.H. Ridouane, A. Campo, M. Hasnaoui, Turbulent natural convection in an air-filled isosceles triangular enclosure, Int. J. Heat Fluid Flow 27 (2006) 476–489.